Morphological Profiles Based on Differently Shaped Structuring Elements for Classification of Images With Very High Spatial Resolution

Zhi Yong Lv, Penglin Zhang, Jon Atli Benediktsson, *Fellow, IEEE,* and Wen Zhong Shi

***Abstract*—Morphological profiles (MPs) have been proposed for the segmentation and classification of high spatial resolution (HSR) images. A shortcoming of the originally proposed MPs is that the profiles were only based on structuring elements (SEs) of one particular shape, suggesting that such MPs may not be suitable for detecting different shapes in images. To better fit several shapes in a given image, a new approach based on mathematical morphology is proposed to extract structural information from HSR images and consequently yield new versions of MPs. The classification results for the new MPs are compared with the classification of spatial features extracted with the use of pixel shape index, gray level co-occurrence matrix, and previously proposed MPs. The experimental results suggest the following: 1) structural and spectral features can complement each other and their integration can improve classification accuracy and 2) MPs constructed by differently shaped SEs are less sensitive to salt-and-pepper noise than those constructed by fixed-shaped SEs.**

***Index Terms*—Classification, high spatial resolution (HSR) images, morphological profile (MP), shape of structuring element (SE).**

I. Introduction

AT PRESENT, a large amount of detailed ground information can be acquired because of the increased availability of high spatial resolution (HSR) images in urban areas. Thus, the potential applications of remote sensing have increased; these applications include urban monitoring, decision-making in urban development, and studies on the effects of human activities. The classification of HSR images should be useful in practical applications. However, high geometrical resolution and rich spectral information can result, on the one hand, in images that have different spectral values for the same classes and, on the other hand, in images that show a similar spectral reflectance for different classes. Therefore, the structural or spatial information in HSR image must be exploited to enhance the classification by spectral-based approaches [1]–[3]. This paper develops novel morphological profiles (MPs) based on mathematical morphology for extracting structural information. The proposed MPs are investigated in classification of HSR image data.

Spatial features (or structural information) complement spectral information in classification of HSR image [1], [4], [5], and a number of methods have been proposed for such classification, including spatial feature extraction based on contextual information. This approach extracts the shape, texture, or contextual information from an HSR image on the basis of the contextual relationship among neighboring pixels. In addition, the extracted spatial features are combined with the spectral features for the purpose of classification. Huang *et al.* proposed a spatial feature called pixel shape index (PSI), which describes the shape feature of a local area that surrounds a central pixel on the basis of spectral similarity. Texture is another widely used feature in classification of images because high-resolution images can describe ground texture in detail. The wavelet transform [6] and the gray-level co-occurrence matrix (GLCM) [7] are the most commonly used texture feature extraction methods. In addition, the Markov random field and its derivative approaches can be used to extract spatial features from high-resolution images [8]–[10].

Recently, several approaches based on mathematical morphology have been successfully used in classification of HSR images from urban areas. Benediktsson *et al.* presented differential MPs (DMPs) based on increasing the sizes of structuring elements (SEs) [11] in opening and closing operators. Meanwhile, extended MPs (EMPs) have been proposed for analyzing hyperspectral data [12]. Weighted DMPs were proposed for HSR image classification in [13]. Furthermore, Dalla Mura *et al.* defined morphological attribute profiles (APs), which provide a multilevel characterization of an image created by the sequential application of morphological attribute filters. These filters can be used to model different kinds of structural information [14]. APs were also extended in [15]. Although MP is a powerful tool for investigating the scale of structures in whole image scenes, the practical application of MPs faces two problems. 1) When a single-shaped SE is used to model the spatial information within an image scene, the SE may be unable to cover the multifarious structures in the entire image, even though the suitability of the SE to model the size of an object is enhanced by a set of variable sizes. 2) The selection of the shape of the SE

Manuscript received February 06, 2014; revised April 25, 2014; accepted May 26, 2014. Date of publication July 16, 2014; date of current version January 21, 2015. This work was supported in part by the Project 2012BAJ15B04, in part by the key project of National Natural Science Foundation of China under Grant 41331175, and in part by the National Natural Science Foundation of China under Grant 61202194. *(Corresponding author: Peng Lin Zhang.)*

Z. Y. Lv is with the School of Computer Science and Engineering, Xi'an University of Technology, Xi'an 710048, China.

P. Zhang is with the School of Remote Sensing and Information Engineering, Wuhan University, Wuhan, China (e-mail: zpl@whu.edu.cn).

J. A. Benediktsson is with the Faculty of Electrical and Computer Engineering, University of Iceland, Reykjavik, Iceland.

W. Z. Shi is with the Joint Spatial Information Research Laboratory Between the Hong Kong Polytechnic University and Wuhan University, Wuhan University, Wuhan 430079, China.

Color versions of one or more of the figures in this paper are available online at http://ieeexplore.ieee.org.

Digital Object Identifier 10.1109/JSTARS.2014.2328618

for MPs is another problem because the shape of the SE is crucial for extracting structures from an image. That is, SE is used to probe or interact with a given image, and the result of the extraction depends on how the selected shape fits or misses objects in the image. In particular, the choice of a certain SE for a particular morphological operation influences the information obtained. One of the two main shape characteristics is related to the SE [16]. To date, not much attention has been given to the shape of SEs in the application of MPs. Therefore, the influence of the shape of SEs on the application of MPs needs to be investigated.

In this paper, a novel approach is proposed for constructing MPs that is based on multishaped SEs. Compared with conventional MPs, the proposed approach fits more shapes and extracts more structural information from a given image. To verify the performance of the proposed method, three experiments were designed on the basis of three HSR images: 1) a ROSIS-03 hyperspectral image of Pavia University; 2) a hyperspectral ROSIS-03 scene at Pavia Center; and 3) IKONOS data obtained from Reykjavik, Iceland. In these experiments, the proposed MP-based approach is compared with the approaches that use a spectral feature only along with approaches that use other spatial features, such as EMP-based approaches that have previously been applied in the classification of HSR images from urban areas [12].

This paper is organized as follows. Section II describes the process of constructing MPs based on multishaped SEs. Section III shows the framework of the proposed MPs applied in the classification of HSR images. Section IV details experiments on three HSR data sets. Section V presents the conclusion of this paper.

II. New MPs With Multishaped SEs

Whichever operator of mathematical morphology is applied in image processing, an SE of a well-known shape must be adopted to extract the structural information from an image. An SE is a template composed of a small matrix of pixels, and each pixel has a value of zero or one. The matrix dimensions specify the size of the SE. The patterns of ones and zeros specify the shape of the SE. The SE is centered at all possible locations in the image and is compared to its neighboring pixels.

The basic operators of mathematical morphology are dilation and erosion. Two important operators are based on dilation and erosion: 1) opening and 2) closing. Considering an image X, let x be a pixel in the image, and the domain of X be $\mathbb{R}^n$ [usually, $n = 2$, e.g., a two-dimensional (2-D) image], $\forall x \in \mathbb{R}^n$. The result of an erosion $\Delta_S(X(x))$ of a grayscale image X at pixel x by SE with the shape S is the minimum value of pixels inside S_d (where S_d is the defined domain of S and S is centered at pixel x), as shown in

$$\Delta_S(X(x)) = \min_{x_i}(x_i \in S_d). \tag{1}$$

Dilation ∇ is defined as the dual operator of erosion. Therefore, the minimum operator in the definition of erosion should be switched to the maximum operator in the case of dilation, as shown in

$$\nabla_S(X(x)) = \max_{x_i}(x_i \in S_d). \tag{2}$$

Dilation and erosion are the two fundamental morphological operators. Erosion-based operations test whether an SE "fits" an object within a neighborhood, whereas dilation-based operations test whether an SE "hits" an object in a neighborhood. This means that dilation adds pixels to the boundaries of objects in an image, whereas erosion removes pixels from object boundaries. The number of pixels added or removed from an object depends on the size and shape of SE used to process the image.

A combination of erosion and dilation gives either opening or closing, i.e., the opening ($\gamma_S(X)$) and closing operators ($\phi_S(X)$) are, respectively, defined as

$$\gamma_S(X) = \nabla_S \circ \Delta_S(X) \tag{3}$$

$$\phi_S(X) = \Delta_S \circ \nabla_S(X) \tag{4}$$

where $\circ$, the operation of opening an image, is an erosion followed by a dilation, where the same SE is used for both operations. The closing of an image is the reverse, as it consists of a dilation followed by an erosion with the same SE.

On the one hand, the basic effect of opening is fairly similar to that of erosion, in that opening tends to remove bright pixels from a fitted object. On the other hand, closing is similar to dilation, in that closing tends to enlarge the boundaries of foreground regions in an object but is less destructive to the shape of the object being processed.

When mathematical morphology is used to extract structures, the response for a given SE depends on the interaction between the shape and size of the SE and the objective structure. The shape of structures is difficult to detect in practical applications. In other words, a prior-SE is impossible to determine accurately. The shape is usually chosen on the basis of some *a priori* knowledge regarding the geometry of the relevant and irrelevant image structures. Thus, MPs based on a range of different SE shapes should be used to cover a greater number of different structures in the spatial domain and to obtain the best response of the structure during image processing.

In view of the proposed notion of morphological characteristics, a novel MP with differently shaped SEs is proposed in this study. The definition of the proposed MP is based on the opening and closing operations. A family of shapes, $S = \{S_1, S_2, S_3, \ldots, S_n, n = 1, 2, 3, \ldots\}$, is considered. Let S_n be the shape of an SE with a fixed size, and n be the total number of shapes considered for an SE. Let X be an image. Thus, the proposed MPs with differently shaped SEs are defined as the composition of profiles built with the opening and closing operations. This composition is built by reconstruction with the use of SEs with different shapes but of the same sizes

$$MP^{(2n+1)}(X) = [\phi^{(n)}_{S_n}(X), \ldots, \phi^{(1)}_{S_1}(X), X \; \gamma^{(1)}_{S_1}(X), \ldots, \gamma^{(n)}_{S_n}(X)]. \tag{5}$$

From a single panchromatic image, the MPs with n-shaped SE results in a $2n + 1$ band image. An example of the proposed MPs with three differently shaped SEs, based on a single band image, is given in Fig. 1.

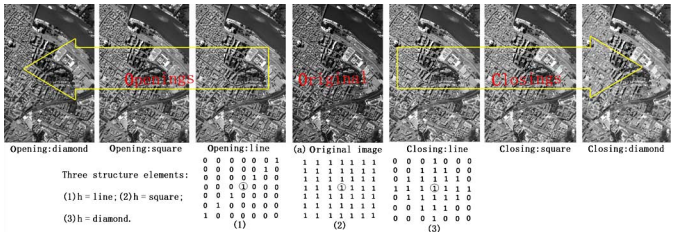

Fig. 1. MPs based on differently shaped SEs (three opening and three closing operations); the fixed size of each SE is 3×3.

In this paper, each pixel (x_i) from the image (X) is processed by both opening and closing operations to extract the fitted structure in the image. Different shapes of the SE have a fixed size centered at pixel x_i to improve the likelihood that the SE would fit the structure in the image. From a theoretical viewpoint, the spatial information of the geometric features can be analyzed by using a set of MPs, which are generated by the repeated use of the opening and closing operations with a set of differently shaped SEs. An original gray-level image of MPs based on three shapes (line, square, and diamond) is presented as an example in Fig. 1.

III. Proposed MPs-Based Classification System

As demonstrated by previous studies [1], [3], [8], extraction of spatial features is helpful in the classification of HSR images. A schematic of a classification system based on the proposed MPs is shown in Fig. 2. The system consists of the following steps.

1) Decomposition is performed because it is necessary in the classification of high-resolution and hyperspectral data. For panchromatic images (one-band images), the approach is applied directly to the single band. In contrast, to apply the MPs on a hyperspectral image, a characteristic image needs to be extracted from the original data [12] by a decomposition approach, such as principal component analysis (PCA) [17] or independent component analysis (ICA) [18]. In this paper, PCA was adopted to extract the principal components, which are given as $PC = \{pc_1, pc_2, pc_3, \ldots, pc_i\}$, where i is the number of principal components. The approach detailed in [12] was used in determining the number of principal components selected from PC for consideration during the construction of the proposed MPs.
2) A set of differently shaped SEs was used to construct the MPs by repeating the opening and closing operations on the selected PC components. For example, if an SE with 3 different shapes was adopted and 3 components were selected, an 18 dimensional profile would then be created for the original image.
3) The proposed MPs and the selected spectral principal components were then integrated by using a layer-stacking tool embedded in the ENVI 4.8 business software.
4) The support vector machine (SVM) [19] classifier was used in the classification of the spectral and structural features provided by the proposed MPs.

Finally, the accuracy of the entire procedure was assessed.

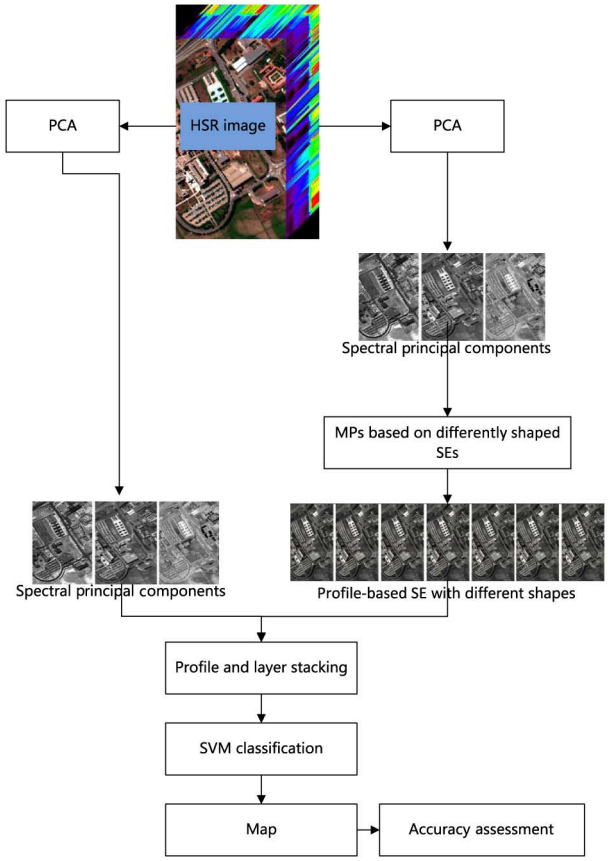

Fig. 2. Classification system based on the proposed MPs applied to hyperspectral.

IV. Experiments and Analysis

In this section, the proposed MPs were tested in the classification of HRS data in three experiments using two HRS hyperspectral images and one HRS panchromatic image. The two hyperspectral images were acquired with the ROSIS-03 sensor during a flight campaign over Pavia in northern Italy. The ROSIS-03 sensor produced 115 data channels, with a spectral coverage ranging from 0.43 to 0.86 μm. The ROSIS-03 has a 1.3-m spatial resolution. The panchromatic image obtained by the IKONOS satellite has a 1.0-m spatial resolution. Each of the three experiments is detailed in Section IV.

In the following experiments, SVM with radial basis function (RBF) function are adopted as classifier for each image to ensure comparing fairness. RBF works well in most cases, and there are two parameters for an RBF kernel, i.e., the Gamma and the penalty parameter. It is not known beforehand which Gamma and penalty parameter are the best for a given image. Consequently, some kind of parameter estimation must be done. The goal is to identify good parameters (Gamma and penalty parameter) in order for the SVM to accurately classify unknown data (i.e., test data). Cross-validation (CV) is widely used to achieve this goal. In v-fold CV, a training set is divided into v subsets of equal size. Sequentially, one subset is tested using the classifier trained on the remaining $v-1$ subsets. Thus, each instance of the whole training set is predicted once

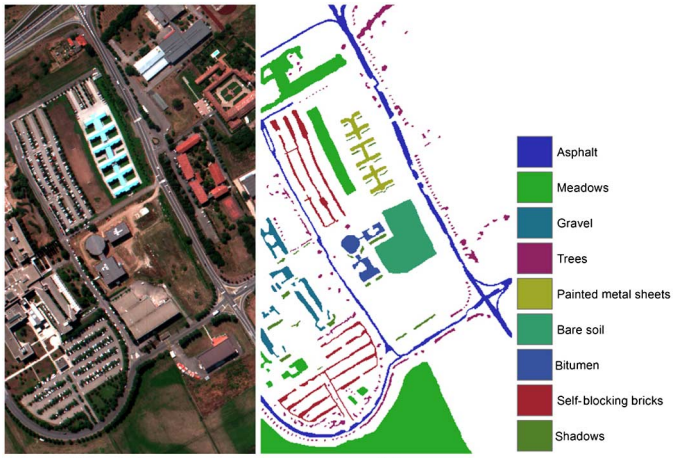

Fig. 3. False color original image of the university area (channels 60, 27, and 17 for RGB, respectively) and the ground reference samples.

TABLE I
TRAINING AND TEST SET FOR THE PAVIA UNIVERSITY IMAGE

Class		Samples	
No.	Name	Training	Test
1	Asphalt	96	6631
2	Meadows	100	18 649
3	Gravel	45	2099
4	Trees	46	3064
5	Painted metal sheets	46	1345
6	Bare soil	97	5029
7	Bitumen	24	1330
8	Self-blocking bricks	51	3682
9	Shadows	36	947
Total		541	42 776

so the CV accuracy is the percentage of data that are correctly classified. The CV procedure can prevent overfitting. Therefore, CV is used for parameter selection in the following experiments, and the default v is set as 5.

A. Experiment 1: ROSIS-03 Pavia University Image

This experiment has two purposes. The first purpose is to test the effectiveness of the proposed MPs in extracting structure information. The second purpose is to explore whether the combination of the spatial features extracted by the proposed MPs and the spectral features can perform well in HSR data classification. The proposed MPs are compared with the classification of the spectral feature alone and other approaches that use spatial information, i.e., PSI [2], GLCM [7], and EMPs [12]. The original data set is 610×340 pixels. A total of 12 channels were removed because of noise. The remaining 103 spectral dimensions were processed. Nine classes of interest were considered: Trees, asphalt, bitumen, gravel, painted metal sheets, shadows, bricks, meadows, and soil. A false color composite of the image with channels 60, 27, and 17 for red, green, and blue, respectively, is shown in Fig. 3(a). The ground reference samples are shown in Fig. 3(b).

In this experiment, a hyperspectral image was classified. Therefore, the dimensionality of the spectral information needs to be reduced for the mathematical morphological approaches prior to processing. The top three principal components ($pc_1, pc_2,$ and pc_3) were selected from 103 bands by using PCA. These top components accounted for approximately 98.86% of the total variance in the image. To test the effectiveness of the proposed MPs coupled with spectral information in the classification, the spectral feature [20] and three other spatial features [2], [7], [12] were compared with the proposed MPs using the same training and test data. The details of the training and test samples are listed in Table I. The parameters for each approach are detailed as follows.

1) *Spectral feature:* The top three principal components were placed into the SVM classifier as spectral features for classification. A RBF kernel function was used, and the parameters were set by CV. The obtained Gamma parameter was 0.33, and the penalty parameter was 100.0.
2) *PSI:* This feature was extracted according to [2], and the three parameters ($T_1 = 50$, $T_2 = 100$, and $D = 20$) were selected. PSI coupled with spectral feature were used for classification, and the parameters (Gamma: 0.5, penalty parameter: 100.0) of the SVM with the RBF kernel were acquired through CV.
3) *GLCM:* The "mean, variance, homogeneity, and correlation" of GLCM were computed from the top three principal components with a 3×3 window. These textural and spectral features were used for classification based on SVM with RBF. The parameters (Gamma: 0.2, penalty parameter: 100.0) of SVM with the RBF kernel were acquired through CV.
4) *The parameters of EMPs [12]:* SE is a "disk" with an increasing size: 2×2, 4×4, 6×6, and 8×8. The EMPs were constructed through a repeated use of the opening and closing operations by SEs with increasing sizes. The parameters (Gamma: 0.143, penalty parameter: 100.0) of SVM with the RBF kernel were acquired through CV.
5) The proposed MPs were constructed by differently shaped SEs. The shape set used for SE was $S = \{s : s = 'disk', 'line', 'square', 'diamond'\}$ with a fixed size of 4×4 pixels. Each shape of the SE was used twice, i.e., for one opening operation and one closing operation, to extract structural information. For example, a disk-shaped SE with a size of 4×4 pixels was used to construct two profiles (one opening profile and one closing profile) through the opening and closing operations, starting with one spectral component (e.g., pc_1). Thus, the proposed MPs were constructed through the repeated use of the closing and opening operations of the SEs with different shapes and a fixed size. The proposed MPs were then coupled with spectral features for classification. The SVM classifier with RBF was adopted, and the parameters for SVM with the RBF kernel were obtained through CV. The Gamma parameter was 0.111, and the penalty parameter was 100.0.

TABLE II
CLASS-SPECIFIC ACCURACIES (%) FOR DIFFERENT FEATURE SETS IN SVM CLASSIFICATION OF THE PAVIA UNIVERSITY IMAGE

Class	Spectral feature only	PSI	GLCM	EMPs	Proposed MPs
Asphalt	79.9	86.4	89.5	87.0	89.9
Meadows	69.9	81.2	74.5	91.3	92.5
Gravel	63.1	54.1	56.2	74.3	76.0
Trees	78.8	85.3	94.5	97.8	93.9
Painted metal sheets	99.5	99.4	98.4	99.8	99.7
Bare soil	37.7	49.7	59.5	68.6	54.8
Bitumen	45.2	45.1	67.6	63.4	78.0
Self-blocking bricks	56.1	65.3	74.1	93.5	69.4
Shadows	99.8	99.6	93.5	98.5	98.6
OA	67.6	75.8	76.5	87.3	84.9
AA	70.0	74.9	77.5	86.0	83.6
Ka	0.58	0.682	0.697	0.832	0.799

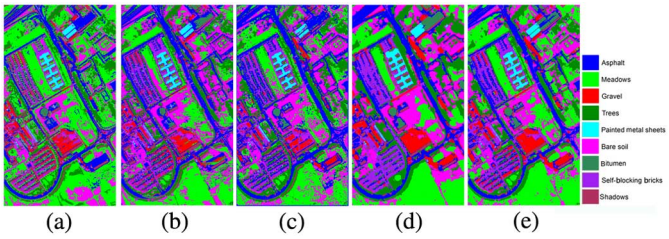

Fig. 4. Classification maps obtained for different feature types of the Pavia University image: (a) spectral feature only; (b) PSI feature; (c) GLCM (mean, variance, homogeneity, and correlation); (d) EMPs suggested in [12]; and (e) the proposed MPs.

In view of the above-mentioned parameter settings, the proposed MPs were evaluated and compared to other approaches. Class-specific accuracies for different approaches are listed in Table II, and the visual classification maps are shown in Fig. 4. The spectral feature coupled with the proposed MPs exhibited an overall accuracy (OA) of 84.9%, an average accuracy (AA) of 83.6%, and a kappa coefficient (Ka) of 0.799. As demonstrated in Table II, these accuracies were higher than the ones obtained with the use of spectral features only, which had an OA of 67.6%, an AA of 70.0%, and a Ka of 0.58. Compared with PSI and GLCM, the proposed MPs also exhibited superior OA, AA, and Ka. The best classification rates for *Meadows*, *Gravel,* and *Bitumen* were achieved through the proposed MPs. These elements (*Meadows*, *Gravel*, and *Bitumen*) typically have ambiguous and uncertain shapes in HSR images. However, the proposed MPs improved the probability of the "SE hitting the shapes in the image" because of the greater number of different shapes of SEs. Furthermore, the proposed MPs achieved an OA and Ka that are similar to those from EMPs suggested in [12].

The experimental results showed that the proposed MPs are effective for structural information extraction. In comparison with PSI and GLCM, the proposed MPs can increase the classification accuracies of OA, AA, and Ka. In addition, the proposed MPs can obtain similar accuracies with EMPs suggested in [12]. Fig. 4 shows the classification map of each method. As shown in Fig. 4, the pure spectral feature cannot effectively discriminate between spectrally similar objects such as *Meadows* and *Trees*.

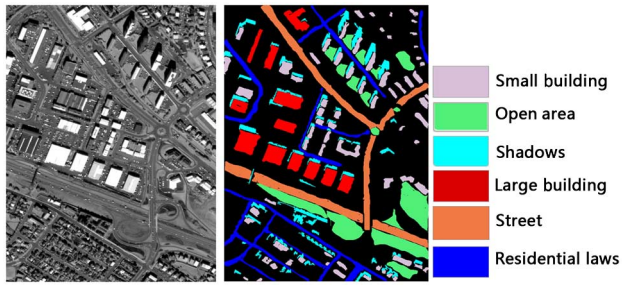

Fig. 5. IKONOS panchromatic image from Reykjavik, Iceland, and the available ground reference samples.

TABLE III
TRAINING AND TEST SAMPLES FOR THE IKONOS REYKJAVIK IMAGE

Class		Samples	
No.	Name	Training	Ground reference
1	Small buildings	1526	34 155
2	Open areas	7536	25 806
3	Shadows	1286	43 867
4	Large buildings	2797	39 202
5	Streets	3336	30 916
6	Residential lawns	5616	35 147
Total		22 097	209 093

B. Experiment 2: IKONOS Panchromatic Image From Reykjavik, Iceland

An IKONOS image from Reykjavik, Iceland, was used in this experiment to illustrate the use of the proposed approach for panchromatic images. The IKONOS image is a high-resolution panchromatic image with a spectral coverage from 0.45 to $0.90\ \mu\text{m}$. Six classes were considered in this case: small buildings, open areas, shadows, large buildings, streets, and residential lawns. The IKONOS image had 975×639 pixels, with a 1.0-m spatial resolution. The original data and the available ground reference data are shown in Fig. 5.

The training samples were selected randomly. The training and test pixels in each class are detailed in Table III, and the available reference data are shown in Fig. 5. In addition, the parameters in this experiment were set as follows: T_1 was 20, T_2 was 50, and the D of the PSI was 20. GLCM was computed using a 3×3 pixel window. The shape family of the SE for the proposed MPs is $S = \{s : s = 'disk', 'line', 'square', 'diamond'\}$, with a fixed size of 8×8 pixels. For the "disk" shape, the SE of the EMPs increased from 2 to 8. Finally, the parameters of the SVM with the RBF kernels were optimized through CV.

The class-specific accuracies are shown in Table IV, and the visual classification maps are shown in Fig. 6. Here, as opposed

TABLE IV
CLASS-SPECIFIC ACCURACIES (%) FOR DIFFERENT FEATURE SETS IN SVM CLASSIFICATION OF THE IKONOS DATA FROM REYKJAVIK

Class	Spectral feature only	PSI	GLCM	EMPs	Proposed MPs
Small building	20.2	39.8	35.5	49.4	53.3
Open area	67.4	61.3	61.0	54.6	52.3
Shadows	89.0	89.3	96.3	87.5	87.4
Large building	43.1	27.0	35.5	37.3	55.6
Street	14.6	20.2	34.1	69.1	73.5
Residential lawns	66.0	73.1	62.2	64.2	67.5
OA	48.6	50.5	52.6	59.6	63.8
AA	50.5	51.8	54.1	60.35	64.9
Ka	0.377	0.4	0.427	0.512	0.563

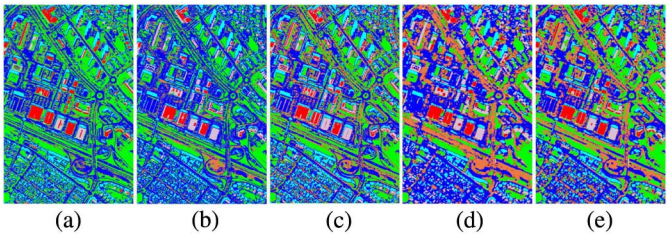

Fig. 6. Classification maps obtained through the SVM classification of the IKONOS panchromatic image from Reykjavik, Iceland: (a) spectral feature only; (b) PSI feature; (c) GLCM (mean, variance, homogeneity, and correlation); (d) conventional MPs suggested in [12]; and (e) the proposed MPs.

to the previous experiment, we do not consider the EMPs for comparison because the data are panchromatic. Therefore, the proposed approach is compared with the original MPs that were proposed for panchromatic images. The MP approach proposed here obtained the highest accuracies for most classes and acquired the highest accuracies for all methods in terms of OA, AA, and Ka. Therefore, the proposed MPs can exploit the rich spatial and structural information in HSR images and are suitable for classifying HSR panchromatic data.

C. Experiment 3: ROSIS-03 Pavia Center Image

The false color image of the data is shown in Fig. 7(a), with channels 60, 27, and 17 for red, green, and blue, respectively. The Pavia Center image was originally 1096×1096 pixels. A 381 pixel-wide black strip was processed, resulting in a "two-part" 1096×715 pixel image. The ground reference map is shown in Fig. 7(b). For the classification, nine classes were defined: water, trees, meadows, bricks, soil, asphalt, bitumen, tiles, and shadows. In addition, the training and test samples are detailed in Table V.

To verify that the proposed MPs are robust in classification of HSR images, the performance of the proposed MPs and the previously proposed EMPs [12] were compared with different levels of noise for the HSR image from the Pavia Center. The

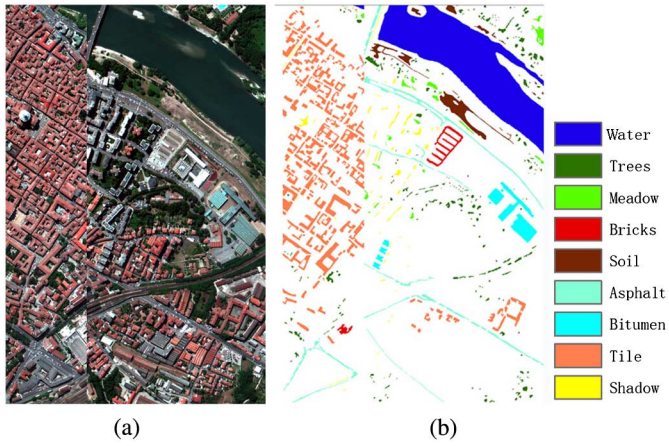

Fig. 7. (a) False color original image of the Pavia Center and (b) the available ground reference samples.

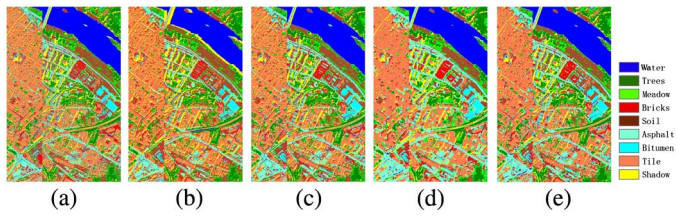

Fig. 8. (a) Classification maps obtained by SVM classification of (a) spectral feature only; (b) PSI feature; (c) GLCM (mean, variance, homogeneity, and correlation); (d) EMPs suggested in [12]; and (e) the MPs proposed in this paper.

TABLE V
TRAINING AND TEST SAMPLES FOR THE PAVIA CENTER IMAGE

Class		Samples	
No.	Name	Training	Test
1	Water	623	65 971
2	Trees	336	7598
3	Meadows	93	3090
4	Bricks	282	2685
5	Soil	241	6584
6	Asphalt	319	9248
7	Bitumen	221	7287
8	Tiles	611	42 826
9	Shadows	359	2863
Total		3085	148 152

top three components (3-pc_s) that accounted for around 99.12% of the total variance of the entire HSR image were used as basic images for the MPs. A false color composite image of the Pavia Center data is shown in the top left corner of Fig. 9 (pc_1 for red, pc_2 for green, and pc_3 for blue). These (3-pc_s) were considered as input features for noise simulations and classification. The principle of determining parameters in this experiment was the same as that in experiment 1 (Pavia University): T_1 was 50, T_2 was 100, and the D for PSI was 20. GLCM was defined by a

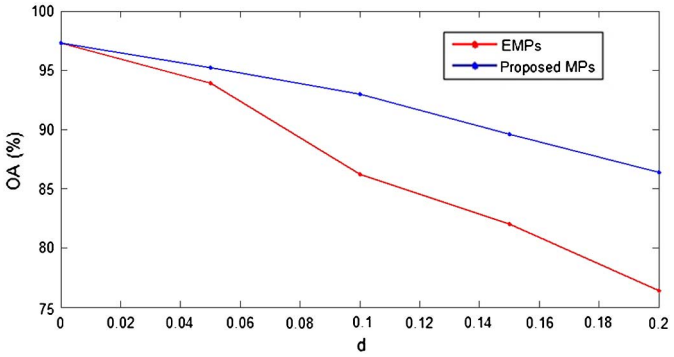

Fig. 9. Pavia Center data: relationship between the OA and the noise density (d) for the EMPs and the proposed MPs.

TABLE VI
CLASS-SPECIFIC ACCURACIES (%) FOR DIFFERENT FEATURE SETS IN THE SVM CLASSIFICATION OF THE PAVIA CENTER DATA

Class	Spectral feature only	PSI	GLCM	EMPs	Proposed MPs
Water	99.7	98.7	99.2	99.9	99.8
Trees	92.1	90.5	94.9	92.2	94.2
Meadows	64.2	62.4	77.5	78.3	78.3
Bricks	55	59.2	68.2	75.3	70.6
Soil	94.4	89.2	95.1	96.2	97.7
Asphalt	95.5	95.4	95.2	98.6	98
Bitumen	80.6	79.3	81.7	80.1	80.8
Tiles	98.1	98.3	99	99.6	99.5
Shadows	99.8	99.7	99.8	96.4	98.1
OA	95.9	95.1	96.6	97.3	97.3
AA	86.6	85.86	90.07	90.7	90.8
Ka	0.942	0.931	0.952	0.961	0.962

3×3 window; EMPs was computed by the disk SEs with the sizes from 2 to 8; and the parameter of SVM with RBF used for each classification was optimized through CV. Based on these parameters' setting, the visual classification maps for Pavia Centre University are shown in the Fig. 8.

In addition, the 3-pc_s false color image was corrupted by "salt-and-pepper" noise with different densities (d) in noise simulations. The salt-and-pepper noise in the image is represented by randomly occurring white and black pixels. In remote sensing applications, salt-and-pepper noise creeps into images in situations where quick transitions, such as faulty switching, occur. The salt-and-pepper noise in this experiment affected approximately $d \times Num(X)$ pixels, where $Num(X)$ is the number of pixels in image X, and the noise is distributed randomly over the image X.

The accuracies of each class are compared in Table VI. It can be observed that the proposed MPs obtained the highest accuracies in terms of OA, AA, and Ka, i.e., when compared to using the spectral feature alone, PSI and GLCM. The proposed MPs and the previously proposed EMPs obtained similar accuracies for all the information classes based on the same training and test samples, and the 3-pc_s were uncorrupted by salt-and-pepper noise. However, when the 3-pc_s were corrupted by salt-and-pepper noise, the proposed MPs obtained higher accuracies than the previously proposed EMPs. A quantitative comparison is presented in Table VII, which shows that the accuracies of the previously suggested EMPs and the proposed MPs decrease when the noise density increases, as shown in Figs. 9 and 10. However, classification accuracies based on the proposed MPs are higher than those of EMPs at the same noise density. Comparisons among the visual results indicate that the proposed MPs present a better classification map than the EMPs with an increasing level of noise, as shown in Fig. 11.

TABLE VII
COMPARISON OF THE CLASSIFICATION ACCURACIES BETWEEN EMPS AND THE PROPOSED MPS WITH DIFFERENT LEVELS OF NOISE IN THE PAVIA CENTER DATA

	EMPs		Proposed MPs	
Noise density (d)	OA (%)	Ka	OA (%)	Ka
0.0	97.3	0.961	97.3	0.962
0.05	93.9	0.915	95.2	0.932
0.1	86.2	0.809	93.0	0.902
0.15	82.0	0.752	89.6	0.854
0.2	76.4	0.68	86.4	0.812

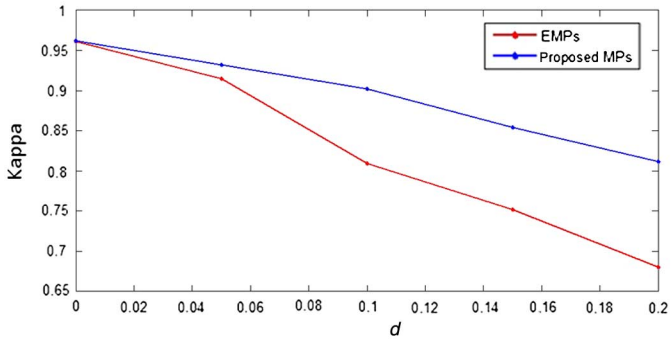

Fig. 10. Pavia Center data: relationship between the kappa coefficient and the noise density (d) for the EMPs and the proposed MPs.

The adaptability of the proposed approach was tested by using a Neural Net (NN) classifier based on the backpropogation scheme and compare it with the performance of the previously obtained classification accuracies of the SVM classifier for the three images (Pavia University, IKONOS panchromatic Reykjavik, and Pavia Center). The same final features are used to feed the NN and the SVM in the previous experiments. The results are shown as Table VIII. Based on the results, It can be determined that the structuring feature extracted by the proposed approach achieves high classification accuracies regardless whether the NN or the SVM are used for classification. The SVM classifier outperformed the NN classifier in terms of accuracies for the three images (Pavia University, IKONOS panchromatic Reykjavik, and Pavia Center).

The results mentioned above show that the proposed MPs are not only effective as a structure extraction approach for HSR data, which can complement the spectral features to enhance the classification accuracy, but the proposed approach also performs better than EMPs [12] in terms of classification accuracies when noise levels are increased.

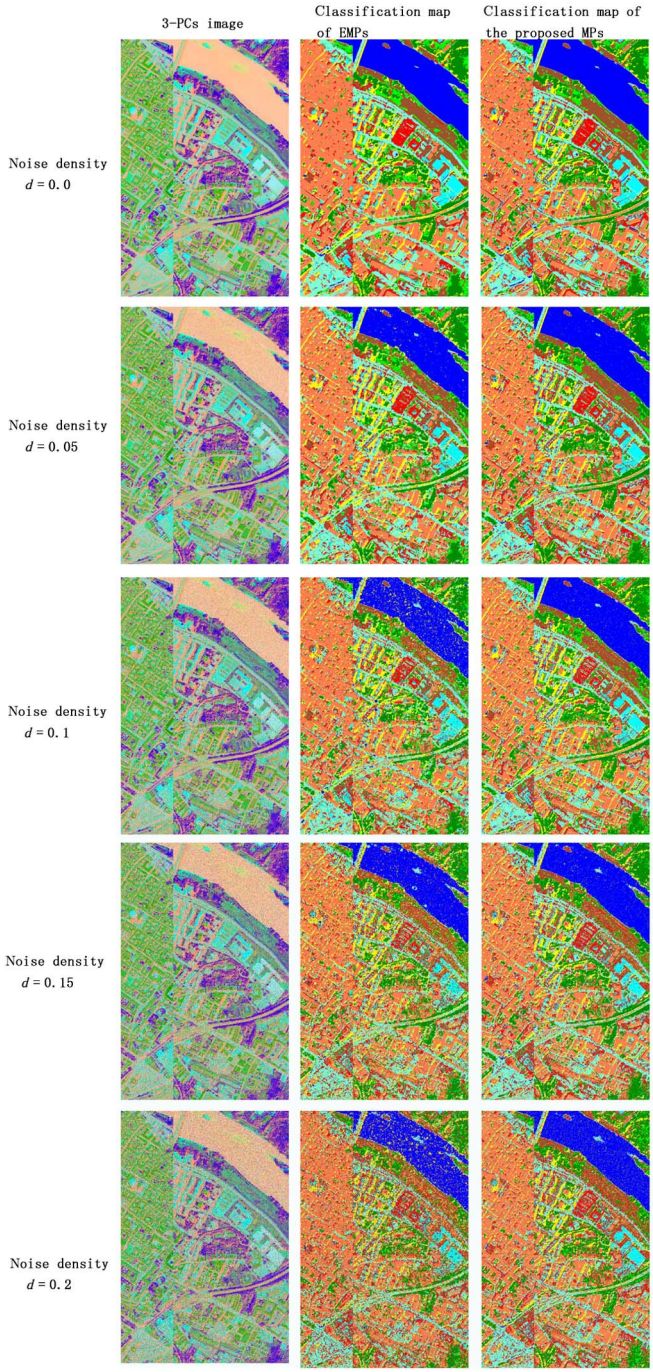

Fig. 11. Visual comparison of the classification maps between EMPs and the proposed MPs with different levels of noise in the Pavia Center data.

TABLE VIII
CLASSIFICATION ACCURACIES (%) FOR THE PROPOSED APPROACH WITH NEURAL NET CLASSIFIER BASED ON THREE HSR IMAGES

	Pavia University image	IKONOS2 Pan image	Pavia Center image
OA (%)	79.0	61.0	95.8
AA (%)	68.2	63.3	89.7
Ka	0.721	0.53	0.941

V. CONCLUSION

A novel approach, which is an extension of the original MPs, is proposed in this paper for the classification of HSR images. This approach was applied in three experiments using two ROSIS-03 hyperspectral images and an IKONOS panchromatic image. The results were then compared with those from other approaches that used other spatial feature extraction techniques, including the previously proposed MPs. The SVM classifier was used in all cases for classification. In summary, the results of the experiments revealed the following.

1) The proposed MPs, which were based on SEs with multiple shapes, are effective for the extraction of structural information from HSR images. The experimental results show that the approach, when coupled with spectral information, is well suited for the classification of HSR data.
2) The proposed MPs perform better than the previously proposed EMPs [12] in terms of classification accuracies with increased levels of noise. MPs constructed by SEs with multiple shapes are less sensitive to salt-and-pepper noise than those that are constructed by SEs with fixed shapes but increasing sizes.

As a topic of future research, another possible approach (multiple SEs with multiple sizes) can also be considered. In theory, the advantage of such an approach may be more effective than that of the proposed approach (multiple SEs with fixed size) for structure extraction. On the other hand, the drawback of such an approach would be the difficulty to decide the best size and the best shape of each SE.

ACKNOWLEDGMENT

The authors would like to thank Prof. P. Gama and Prof. F. DellAcqua of the University of Pavia for kindly providing the ROSIS-03 data sets and the ground reference data. They would also like to thank Prof. M. Dalla Mura, GIPSA-Lab (Grenoble Images Parole Signal Automatique Lab), INPG, Grenoble, France, for his helpful suggestions in improving this paper.

REFERENCES

[1] F. Dell'Acqua *et al.*, "Exploiting spectral and spatial information in hyperspectral urban data with high resolution," *IEEE Geosci. Remote Sens. Lett.*, vol. 1, no. 4, pp. 322–326, Oct. 2004.
[2] L. Zhang, X. Huang, B. Huang, and P. Li, "A pixel shape index coupled with spectral information for classification of high spatial resolution remotely sensed imagery," *IEEE Trans. Geosci. Remote Sens.*, vol. 44, no. 10, pp. 2950–2961, Oct. 2006.
[3] L. Bruzzone and L. Carlin, "A multilevel context-based system for classification of very high spatial resolution images," *IEEE Trans. Geosci. Remote Sens.*, vol. 44, no. 9, pp. 2587–2600, Sep. 2006.
[4] Y. Tarabalka, J. A. Benediktsson, and J. Chanussot, "Spectral spatial classification of hyperspectral imagery based on partitional clustering techniques," *IEEE Trans. Geosci. Remote Sens.*, vol. 47, no. 8, pp. 2973–2987, Aug. 2009.
[5] X. Huang, L. Zhang, and P. Li, "Classification and extraction of spatial features in urban areas using high-resolution multispectral imagery," *IEEE Geosci. Remote Sens. Lett.*, vol. 4, no. 2, pp. 260–264, Apr. 2007.
[6] T. Celik and T. Tjahjadi, "Multiscale texture classification using dual-tree complex wavelet transform," *Pattern Recognit. Lett.*, vol. 30, no. 3, pp. 331–339, 2009.
[7] X. Huang, L. Zhang, and L. Wang, "Evaluation of morphological texture features for mangrove forest mapping and species discrimination using multispectral IKONOS imagery," *IEEE Geosci. Remote Sens. Lett.*, vol. 6, no. 3, pp. 393–397, Jul. 2009.
[8] Y. Zhao, L. Zhang, P. Li, and B. Huang, "Classification of high spatial resolution imagery using improved Gaussian Markov random-field-based texture features," *IEEE Trans. Geosci. Remote Sens.*, vol. 45, no. 5, pp. 1458–1468, May 2007.

[9] G. Rellier, X. Descombes, F. Falzon, and J. Zerubia, "Texture feature analysis using a Gauss–Markov model in hyperspectral image classification," *IEEE Trans. Geosci. Remote Sens.*, vol. 42, no. 7, pp. 1543–1551, Jul. 2004.
[10] A. Sarkar *et al.*, "Unsupervised and supervised classification of hyperspectral imaging data using projection pursuit and Markov random field segmentation," *Int. J. Remote Sens.*, vol. 33, no. 18, pp. 5799–5818, 2012.
[11] J. A. Benediktsson, M. Pesaresi, and K. Arnason, "Classification and feature extraction for remote sensing images from urban areas based on morphological transformations," *IEEE Trans. Geosci. Remote Sens.*, vol. 41, no. 9, pp. 1940–1949, Sep. 2003.
[12] J. A. Benediktsson, J. A. Palmason, and J. R. Sveinsson, "Classification of hyperspectral data from urban areas based on extended morphological profiles," *IEEE Trans. Geosci. Remote Sens.*, vol. 43, no. 3, pp. 480–491, Mar. 2005.
[13] O. Aytekin, M. Dalla Mura, I. Ulusoy, and J. A. Benediktsson, "Classification of hyperspectral images based on weighted DMPs," in *Proc. IEEE Int. Geosci. Remote Sens. Symp. (IGARSS)*, 2012, pp. 4154–4157.
[14] M. Dalla Mura, J. A. Benediktsson, B. Waske, and L. Bruzzone, "Morphological attribute profiles for the analysis of very high resolution images," *IEEE Trans. Geosci. Remote Sens.*, vol. 48, no. 10, pp. 3747–3762, Oct. 2010.
[15] M. Dalla Mura, J. A. Benediktsson, B. Waske, and L. Bruzzone, "Extended profiles with morphological attribute filters for the analysis of hyperspectral data," *Int. J. Remote Sens.*, vol. 31, no. 22, pp. 5975–5991, 2010.
[16] E. Dougherty, *An Introduction to Morphological Image Processing*. Bellingham, WA, USA: SPIE Opt. Eng. Press, 1992.
[17] Q. Du and J. E. Fowler, "Hyperspectral image compression using jpeg2000 and principal component analysis," *IEEE Geosci. Remote Sens. Lett.*, vol. 4, no. 2, pp. 201–205, Apr. 2007.
[18] C. A. Shah, M. K. Arora, and P. K. Varshney, "Unsupervised classification of hyperspectral data: An ICA mixture model based approach," *Int. J. Remote Sens.*, vol. 25, no. 2, pp. 481–487, 2004.
[19] F. Melgani and L. Bruzzone, "Classification of hyperspectral remote sensing images with support vector machines," *IEEE Trans. Geosci. Remote Sens.*, vol. 42, no. 8, pp. 1778–1790, Aug. 2004.
[20] M. Fauvel, J. A. Benediktsson, J. Chanussot, and J. R. Sveinsson, "Spectral and spatial classification of hyperspectral data using SVMs and morphological profiles," *IEEE Trans. Geosci. Remote Sens.*, vol. 46, no. 11, pp. 3804–3814, Nov. 2008.

Zhi Yong Lv received the B.S. degree in computer science and technology from Xinyang Normal University, HeNan, China, in 2006, the M.S. degree from the School of Remote Sensing and Information Engineering, Wuhan University, Wuhan, China, in 2008, and the Ph.D. degree from Wuhan University, in 2014, both in cartography and geography information system.

He worked as an Engineer of surveying with The First Institute of Photogrammetry and Remote Sensing, Xi'an, China, from 2008 to 2011. His research interests include multihyperspectral and high-resolution remotely sensed image processing, spatial feature extraction, neural networks, pattern recognition, and remote sensing applications.

Penglin Zhang was born in 1970. He received the M.S. degree from the School of News and Communication, Wuhan University, Wuhan, China, and the Ph. D. degree from the School of Remote Sensing and Information Engineering, Wuhan University.

Between 1994 and 2003, he was a Lecturer and Assistant Professor with the Wuhan University. Currently, he is an Associate Professor with the Remote Sensing and Information Engineering, Wuhan University. Moreover, as a post doctoral Researcher Fellow, he worked with the Department of Science and Engineering, Ritsumeikan University, Kyoto, Japan, from April 2006 to March 2008; as a Senior Visiting Fellow to visit the Department of Land Surveying and Geo-Informatics, The Hong Kong Polytechnic University, Hong Kong from December 2011 to March 2012. He has published more than 20 research papers in his research fields. His research interests include remote sensing and medical image processing, pattern recognition, image feature extraction, registration and deformation measurement, and artificial intelligence.

Jon Atli Benediktsson (S'84–M'90–S'M'99–F'04) received the Cand.Sci. degree in electrical engineering from the University of Iceland, Reykjavik, Iceland, in 1984, and the M.S.E.E. and Ph.D. degrees in electrical engineering from Purdue University, West Lafayette, IN, USA, in 1987 and 1990, respectively.

Currently, he is Pro Rector for Academic Affairs and Professor of Electrical and Computer Engineering with the University of Iceland. He has published extensively in these fields. His research interests include remote sensing, biomedical analysis of signals, pattern recognition, image processing, and signal processing.

Prof. Benediktsson is a member of the Association of Chartered Engineers in Iceland (VFI), Societas Scinetiarum Islandica, and Tau Beta Pi. He is a Fellow of SPIE. He was the 2011–2012 President of the IEEE Geoscience and Remote Sensing Society (GRSS) and has been on the GRSS AdCom since 2000. He was an Editor of the IEEE TRANSACTIONS ON GEOSCIENCE AND REMOTE SENSING (TGRS) from 2003 to 2008 and served as an Associate Editor of TGRS since 1999, the IEEE Geoscience and Remote Sensing Letters since 2003, and IEEE Access since 2013. He is on the International Editorial Board of the *International Journal of Image and Data Fusion* and was the Chairman of the Steering Committee of IEEE Journal of Selected Topics in Applied Earth Observations and Remote Sensing (J-STARS) 2007–2010. He is a Cofounder of the biomedical startup company Oxymap (www.oxymap.com). He received the Stevan J. Kristof Award from Purdue University in 1991 as outstanding graduate student in remote sensing. In 1997, he was the recipient of the Icelandic Research Council's Outstanding Young Researcher Award; in 2000, he was granted the IEEE Third Millennium Medal; in 2004, he was a corecipient of the University of Iceland's Technology Innovation Award; in 2006, he received the yearly research award from the Engineering Research Institute of the University of Iceland; and in 2007, he received the Outstanding Service Award from the IEEE Geoscience and Remote Sensing Society. He was a corecipient of the 2012 IEEE TRANSACTIONS ON GEOSCIENCE AND REMOTE SENSING Paper Award, and in 2013, he was a corecipient of the IEEE GRSS Highest Impact Paper Award. In 2013, he received the IEEE/VFI Electrical Engineer of the Year Award.

Wen Zhong Shi received the Doctoral degree in photogrammetry and remote sensing from the University of Osnabrueck, Vechta, Germany, in 1994.

He is a Professor in geographic information system (GIS) and remote sensing with the Department of Land Surveying and Geo-Informatics, The Hong Kong Polytechnic University, Hung Hom, Hong Kong, and the Director of Advanced Research Centre for Spatial Information Technology, The Hong Kong Polytechnic University. He is the President (2008–2012) of Technical Commission II of International Society for Photogrammetry and Remote Sensing and served as the President for Hong Kong Geographic Information System Association (2001–2003). He has published over 380 research articles (including over 70 SCI papers) and 10 books. His research interests include GIS, remote sensing, uncertainty and spatial data quality, and image processing for high-resolution satellite images.

Prof. Shi received the State Natural Science Award (Second class) from the State Council of the People's Republic of China, in 2007; ESRI Award for Best Scientific Paper in GIS (the first place recipients) by American Society of Photogrammetry and Remote Sensing, in 2006; Distinguished Young Scholar Fund (B), National Natural Science Foundation, China, in 2006; Chang Jiang Scholar (Chair Professor) by Ministry of Education of China, in 2006; Chinese Science and Technology Progress Award in Surveying and Mapping (First Class), in 2005; and The President's Award for Outstanding Performance/Achievement by the Hong Kong Polytechnic University, in 1999.